Journal of Materials Chemistry C

PAPER

View Article Online
View Journal | View Issue

Cite this: J. Mater. Chem. C, 2015, 3, 5268

$Sr_2(OH)_3NO_3$: the first nitrate as a deep UV nonlinear optical material with large SHG responses†

Ling Huang,[ab] Guohong Zou,*[a] Huaqiang Cai,[a] Shichao Wang,[c] Chensheng Lin[c] and Ning Ye*[c]

Received 4th February 2015,
Accepted 18th April 2015

DOI: 10.1039/c5tc00344j

www.rsc.org/MaterialsC

A noncentrosymmetric nitrate, $Sr_2(OH)_3NO_3$, has been obtained using a hydrothermal method. The structure is built up of nine coordinated $SrO_3(OH)_6$ polyhedra and triangular NO_3 groups. The $SrO_3(OH)_6$ polyhedra share their three equatorial oxygen atoms with three separate NO_3 groups to form SrO_3–NO_3 layers, and the layers are linked by the apical oxygen atoms in the third dimension. Owing to its special coordination, $SrO_3(OH)_6$ forces its three neighboring NO_3 groups to arrange into a perfect parallel alignment in the plane to give the maximum contribution to the nonlinear optical effect. Powder second-harmonic generation (SHG) using the Kurtz–Perry technique shows that $Sr_2(OH)_3NO_3$ is type I phase-matchable, and the measured SHG coefficient was 3.6 times that of KH_2PO_4. The result from the UV-vis diffuse reflectance spectroscopy study of the powder samples indicated that the short-wavelength absorption edge was below 200 nm, suggesting that $Sr_2(OH)_3NO_3$ is the first nitrate as a promising deep-UV nonlinear optical material.

Introduction

Deep-UV nonlinear optical (NLO) crystals[1–15] which can produce deep-UV coherent light with wavelengths below 200 nm have become increasingly important and have been attracting more attention owing to their promising applications in advanced instrument development, photolithography, micro-machining, laser cooling and attosecond pulse generation over the past decade. In spite of many reports in the literature, it is a particularly difficult challenge to obtain practically useful materials possessing high NLO coefficients and wide UV transparency, especially those covering the deep-UV region. In the past decades, many efforts have been made to understand the relationship between the compositions, structures, and NLO properties of crystals, which are critical in the development of new NLO crystals.[16,17] The Anionic Group Theory proposed by Chen[18–20] has been very successful in developing NLO crystals of borates in the UV region. And it pointed out that the macroscopic optical responses of the UV and deep-UV NLO borates are dominated by B–O units. For example: $[B_3O_6]^{3-}$ in β-BaB_2O_4 (BBO);[21] $[B_3O_7]^{5-}$ in LiB_3O_5,[22] CsB_3O_5[23] and $CsLiB_6O_{10}$;[24,25] and $[BO_3]^{3-}$ in $KBe_2BO_3F_2$,[26] $SrBe_2BO_7$[27] and $K_2Al_2B_2O_7$;[28] and $[B_4O_9]^{6-}$ in $Li_2B_4O_7$.[29] Among these B–O units, the planar $[BO_3]^{3-}$ anionic group, possessing a moderate birefringence and a large microscopic second-order susceptibility $\beta^{(2)}$, is considered to be the most suitable basic structural unit of NLO crystals for UV and deep-UV light generation. Analogous to the $[BO_3]^{3-}$ group, $[CO_3]^{2-}$ and $[NO_3]^{-}$ anionic groups also have similar planar triangle structures with π-conjugated molecular orbitals, which motivate our interest in finding new NLO materials in carbonates and nitrates. In our previous research, a series of carbonates such as alkaline and alkaline earth fluoride carbonates $MNCO_3F$[30] (M = K, Rb, Cs; N = Ca, Sr, Ba) and $CsPbCO_3F$[31] have been proven to be promising UV or deep-UV NLO materials with potential in practical applications. Then, some relevant carbonate compounds with excellent NLO properties have constantly been discovered.[32–36] However, investigations of $[NO_3]^{-}$-containing materials with NLO properties have scarcely been systematically studied in contrast to the successful exploration of borates and carbonates.[37–43] Even to date, there have been no nitrates which can act as deep-UV NLO materials. Li[44] has calculated that the microscopic second-order susceptibility $\beta^{(2)}$ of the $[NO_3]^{-}$ group is larger than those of the $[BO_3]^{3-}$ and $[CO_3]^{2-}$ groups. So the $[NO_3]^{-}$ anionic group was selected as a basic structural unit to explore deep-UV NLO materials which may be with large SHG responses.

[a] Institute of Chemical Materials and Advanced Materials Research Center, Key Laboratory of Science and Technology on High Energy Laser, China Academy of Engineering Physics, Mianyang, 621900, P. R. China. E-mail: zough@caep.cn
[b] Si Chuan Research Center of New Materials, Chengdu, 610000, P. R. China
[c] Fujian Institute of Research on the Structure of Matter, Key Laboratory of Optoelectronic Materials Chemistry and Physics, Chinese Academy of Sciences, Fuzhou, 350002, P. R. China. E-mail: nye@fjirsm.ac.cn

† Electronic supplementary information (ESI) available: Photograph of crystals, crystallographic data, X-ray powder diffraction patterns, IR spectra, UV absorption spectra, and band structures. CCDC 1035040. For ESI and crystallographic data in CIF or other electronic format see DOI: 10.1039/c5tc00344j

Though the $[NO_3]^-$ group is a suitable basic structural unit of NLO crystals for UV and deep-UV light generation, we do not find a way to arrange them to connect cooperatively in a crystal to give the maximum contribution to a large macroscopic SHG effect rather than canceling out with each other as in centrosymmetric crystals. On the basis of the relationship between the structure and overall NLO properties, there are two approaches for producing large NLO effects: (1) choosing favorable structural units and having them aligned coparallel and (2) increasing the density of the NLO structural units. In this study, we may expect to apply crystal chemistry to the rational design of NLO crystals in the nitrate series. From the structural analysis of known compounds with planar triangle structure anionic groups,[30–31,45] it was found that polygonal pyramid coordination of the counter cations with equatorial M–O bonds, such as MO_n, MO_3F_2 or MO_6F_2 groups, results in a coplanar alignment of the $[AO_3]$ (A = B, C, N) groups in the lattice. In order to ensure high transmission in the UV region, alkali and alkaline earth metals should be chosen as the counter cations because there are no d–d electron or f–f electron transitions in this spectral region. Guided by this idea, a noncentrosymmetric nitrate, $Sr_2(OH)_3NO_3$, was synthesized, which was proved to be a promising deep-UV nonlinear optical material.

Experimental section

Reagents

$Sr(NO_3)_2$ (99%), NaOH (99%), and NH_4NO_3 (99%) were purchased from Sinopharm and used as received.

Synthesis

Crystals of $Sr_2(OH)_3NO_3$ were synthesized *via* the hydrothermal method using $Sr(NO_3)_2$ (1.06 g, 0.005 mol) and deionized H_2O (10 mL) with the addition of 0.1 g (0.0025 mol) NaOH and 0.4 g (0.005 mol) NH_4NO_3, charging in the Teflon autoclave (23 mL), heating at 200 °C for 4 days, and then slowly cooling to ambient temperature at a rate of 3 °C h^{-1}. Colorless and transparent flaky crystals of $Sr_2(OH)_3NO_3$ (Fig. S1 in the ESI†) were obtained in yields of about 72% (on the basis of Sr).

Single crystal X-ray diffraction

Single crystal X-ray diffraction data were collected at room temperature on a New Gemini, Dual, Cu at zero, EosS2 diffractometer. The structure was solved by the direct methods and refined by full-matrix least-squares fitting on F^2 using SHELX-97.[46] All of the structures were verified using the ADDSYM algorithm from the program PLATON,[47] and no higher symmetries were found. Relevant crystallographic data and details of the experimental conditions for $Sr_2(OH)_3NO_3$ are summarized in Table S1 (ESI†). Atomic coordinates and isotropic displacement coefficients are listed in Table 1. Selected bond lengths and angles (deg) for $Sr_2(OH)_3NO_3$ are listed in Table S2 (ESI†).

Table 1 Atomic coordinates and equivalent isotropic displacement parameters for $Sr_2(OH)_3NO_3$. U(eq.) is defined as one-third of the trace of the orthogonalized U_{ij} tensor

Atom	x	y	z	$U_{eq.}$ (Å^2)	BVS
Sr(1)	0.6667	0.3333	0.0000	0.0060(7)	1.999
N(1)	1.0000	0.0000	0.0000	0.0090(5)	4.840
O(1)	1.0000	0.1090(2)	0.0000	0.0230(3)	1.925
O(2)	0.4532(17)	0.4532(17)	0.5000	0.0091(18)	2.195

Powder X-ray diffraction

X-ray diffraction patterns of polycrystalline materials were obtained on a Rigaku Dmax2500 powder X-ray diffractometer by using Cu Kα radiation (λ = 1.540598 Å) at room temperature in the angular range of 2θ = 5–65° with a scan step width of 0.05° and a fixed time of 0.2 s. The powder XRD patterns of the pure samples of $Sr_2(OH)_3NO_3$ showed good agreement with the calculated XRD patterns of the single-crystal models (see Fig. S2 in the ESI†).

Thermal analysis

Thermogravimetric analysis (TGA) was conducted on a Netzsch STA 449C unit. The crystal samples (5–10 mg) were enclosed in Al_2O_3 crucibles and heated from room temperature to 800 °C at a rate of 10 °C min^{-1} under a constant flow of nitrogen gas.

Infrared spectroscopy

IR spectra were recorded on a Magna 750 Fourier transform infrared (FT-IR) spectrometer as KBr pellets in the range of 4000–400 cm^{-1}.

UV-vis diffuse reflectance spectroscopy

The UV-vis diffuse reflection data were recorded at room temperature using a powder sample with $BaSO_4$ as a standard (100% reflectance) on a PerkinElmer Lamda-900 UV/vis/NIR spectrophotometer and scanned at 200–2500 nm. Reflectance spectra were converted to absorbance spectra using the Kubelka–Munk function.[48,49]

Second-harmonic generation

Powder second-harmonic generation (SHG) signals were measured using the method adapted from Kurtz and Perry.[50] Since SHG efficiencies are known to depend strongly on particle size, polycrystalline samples were ground and sieved into the following particle size ranges: 25–45, 45–62, 62–75, 75–109, 109–150 and 150–212 μm. The measurements were performed using a Q-switched Nd:YAG laser at 1064 nm and a frequency doubling at 532 nm, for visible and UV SHG, respectively. To make relevant comparisons with known NLO materials, crystalline KDP and BBO were also ground and sieved into the same particle size ranges and used as the references for visible and UV SHG, respectively. The samples were pressed between glass microscope cover slides and secured with tape in 1 mm thick aluminum holders containing an 8 mm diameter hole. They were then placed in a light-tight box and irradiated using a pulsed laser. A cutoff filter was used to limit background flash-lamp light on the

sample, and an interference filter was used to select the second harmonic for detection using a photomultiplier tube attached to a RIGOL DS1052E 50 MHz oscilloscope. This procedure was then repeated using the standard nonlinear optical materials KDP and BBO, and the ratio of the second-harmonic intensity outputs was calculated. No index-matching fluid was used in any of the experiments.

Computational descriptions

The DFT calculation was performed using the CASTEP module.[51] The norm-conserving pseudopotentials were used to represent the ion cores. The valence electrons of the component elements were treated as H $1s^1$, O $2s^2 2p^4$, N $2s^2 2p^3$, and Sr $4s^2 4p^6 5s^2$. Hydrogen atomic positions of the OH^- groups were obtained by fixed-lattice constant optimization based on the X-ray crystal structure. All subsequent calculations were performed on this optimized geometry. The plane-wave energy cutoff was set as 600 eV. The self-consistent convergence of the total energy was set as 2.0×10^{-6} eV per atom. The *k*-point sampling in the Brilliouin zone was set to be $3 \times 3 \times 4$ according to the Monkhorst–Pack scheme.[52]

Results and discussion

Crystal structure

$Sr_2(OH)_3NO_3$ crystallizes into a hexagonal crystal system with an acentric space group of $P\bar{6}2m$ (no. 189). Such a strontium nitrate hydroxide has been previously reported which was synthesized through high-temperature solid-state reactions in an evacuated quartz ampoule.[53] In this study, we have synthesized it using a mild hydrothermal method and it is easy to grow large single crystals for subsequent practical applications. As shown in Fig. 1, the structure of $Sr_2(OH)_3NO_3$ can be described with $SrO_3(OH)_6$ polyhedra and NO_3 triangular entities. In the structure, the N atom is coordinated to three O atoms to form a planar NO_3 triangle with N–O bond lengths of 1.254(14) Å and O–N–O bond angles of 120.000(1)°. And the Sr atom is coordinated to three O atoms and six hydroxyl groups to form $SrO_3(OH)_6$ polyhedra (Fig. 2). Sr–O bond lengths in the $SrO_3(OH)_6$ polyhedra are

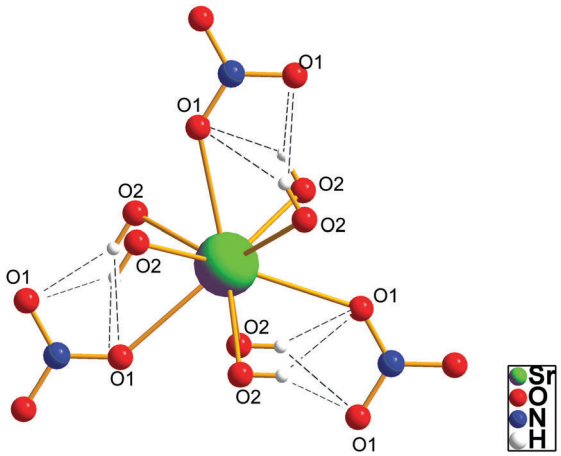

Fig. 2 Alignment of NO_3 groups with the $SrO_3(OH)_6$ polyhedron.

2.6259(13) and 2.7980(10) Å. The inter-atomic distances, 2.953 Å for O1/O2, indicate that strong hydrogen bonds are formed (Fig. 2). So the OH anions in the structure are not only bound to the Sr atoms but also to the N atoms. The $SrO_3(OH)_6$ polyhedra share their three equatorial oxygen atoms with three separate NO_3 groups to form a flat SrO_3–NO_3 layer, and the adjacent layers are linked by the apical oxygen atoms along the *c* direction in the third dimension. Among different layers, the alignment of NO_3 groups is governed by the $SrO_3(OH)_6$ coordination: the nine coordinated atoms to Sr can be divided into three layers, and the steric force of the three central O atoms forces the three above- and three lower-layer O atoms to orient in an eclipse style; also strong hydrogen bonds exist between the three above-and three lower-layer O atoms of six hydroxyl groups and the three central O atoms which force the NO_3 groups to align parallelly in neighboring layers.[54–56] This two-stage alignment of the NO_3 groups produces cooperative contribution to a large macroscopic SHG effect.

The bond valence sums for $Sr_2(OH)_3NO_3$ is calculated using the formula

$$V_i = \sum_j S_{ij} = \sum_j \exp\{(r_0 - r_{ij})/B\} \quad (1)$$

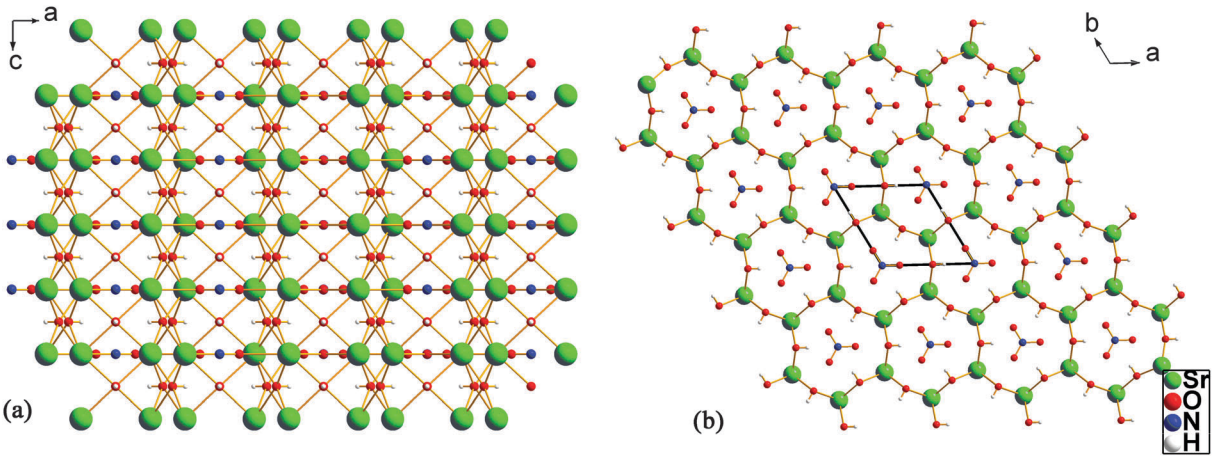

Fig. 1 View of the structure of $Sr_2(OH)_3NO_3$ down the *b* axis (a) and down the *c* axis (b).

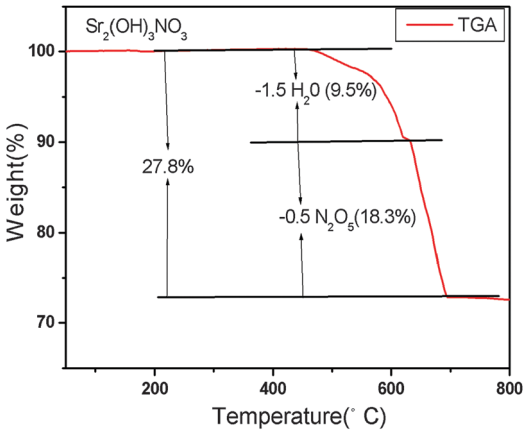

Fig. 3 Thermogravimetric analysis of $Sr_2(OH)_3NO_3$.

where S_{ij} is the bond valence associated with bond length r_{ij} and r_0 and B (usually 0.37) are empirically determined parameters.[21] The calculated total bond valences for Sr, N and O atoms are summarized in Table 1. Both the bond lengths and BVSs for the Sr and N coordinations show that they are close to the ideal values, indicating not only the validity of the structure but also the nonexistence of large strain in the structure.

Thermal properties

The TGA curve (Fig. 3) shows that $Sr_2(OH)_3NO_3$ is stable up to 450 °C and the weight loss undergoes two steps in the range of 450–700 °C under a nitrogen atmosphere, resulting in a total weight loss of about 27.8% (calculated value 28.1%). The first step, with a weight loss of about 9.5% in the range of 450–640 °C, can be assigned to the condensation of 3 hydroxyl groups (calculated value 9.4%). The second step presents a weight loss of about 18.3% (calculated value 18.7%) in the range of 640–700 °C, corresponding to decomposition of one nitrate group. The decomposition reaction is shown below

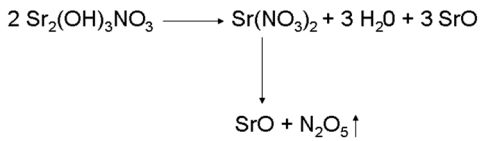

Optical properties

UV-vis diffuse reflectance spectra were collected for the reported compound $Sr_2(OH)_3NO_3$. Absorption (K/S) data were calculated from the following Kubelka–Munk function: $F(R) = (1 - R)^2/2R = K/S$, where R is the reflectance, K is the absorption, and S is the scattering.[48,49] In the (K/S)-*versus*-E plots, extrapolating the linear part of the rising curve to zero provides the onset of absorption. No obvious absorption peak in the range of 6.20–1.55 eV corresponding to 200–800 nm was observed for $Sr_2(OH)_3NO_3$ in Fig. S3 (ESI†). The results indicate that the experimental band gap value of $Sr_2(OH)_3NO_3$ is greater than 6.20 eV, suggesting that $Sr_2(OH)_3NO_3$ may be potentially applied as a deep-UV NLO material.

Fig. S4 (ESI†) presents the IR spectra of $Sr_2(OH)_3NO_3$. Referring to the literature,[42,43] the peaks at around 3500 cm^{-1} can be attributed to the presence of hydroxyl groups. The peaks at 1442, 1394, and 840 cm^{-1} can be attributed to asymmetric stretching and symmetric stretching vibrations of $[NO_3]^-$ groups.

NLO properties

The curves of the SHG signal as a function of particle size of the ground $Sr_2(OH)_3NO_3$ crystals measured using a laser at 1064 nm and 532 nm as the fundamental waves are shown in Fig. 4. A KDP sample was used as the reference for visible SHG, and BBO was used for UV SHG. The results are consistent with phase-matching behavior in both visible and UV regions according to the rule proposed by Kurtz and Perry.[50] The second-harmonic signal is found to be 3.6 × KDP for $Sr_2(OH)_3NO_3$. Since the reported d_{36} coefficient for KDP is 0.39 pm V^{-1},[57] the derived d_{eff} coefficient for $Sr_2(OH)_3NO_3$ is 1.40 pm V^{-1}. The relative magnitude of SHG coefficients in the visible region and that in the UV region are in accordance with each other, considering that the NLO coefficient of BBO is about 4.8 times as large as that of KDP.

According to the anionic group theory,[18,19] the dipole transition from the cations (Sr^{2+} in this case) to the anionic groups ($[NO_3]^-$ in this case) is the off-site transition. Its value is about one order smaller than the dipole transition of the intra-atomic transitions within anionic groups. So the contribution to the main SHG coefficients of $Sr_2(OH)_3NO_3$ from the anionic groups $[NO_3]^-$ is dominant, which is much larger than that of the charge transfer between the s-states of cations and the p-originated states of anions. Therefore the macroscopic second-order susceptibility $\chi^{(2)}$ could be expressed by eqn (2) on the basis of the anionic group theory,

$$x^{(2)}_{ijk} = \frac{F}{V}\sum_{P}\sum_{i'j'k'}\alpha_{ii'}\alpha_{jj'}\alpha_{kk'}\beta^{(2)}_{i'j'k'}(P) \quad P = [NO_3]^- \tag{2}$$

where F is the correction factor of the localized field; V is the volume of the unit cell; $\alpha_{ii'}$, $\alpha_{jj'}$, and $\alpha_{kk'}$ are the direction cosines between the macroscopic coordinates of the crystal and the microscopic coordinates of $[NO_3]^-$ groups, and $\beta^{(2)}_{i'j'k'}$ is the microscopic second-order susceptibility tensor of an individual group. Owing to the fact that $[NO_3]^-$ is a planar group in point group D_{3h}, there are only two nonvanishing second-order susceptibilities $\beta^{(2)}_{111} = \beta^{(2)}_{222}$ in the Kleinman approximation. Because the geometrical factor, g, can be derived from eqn (3), eqn (2) may be simplified according to the deduction process shown in ref. 58:

$$\begin{aligned} x^{(2)}_{ijk} &= \frac{F}{V}\cdot g_{ijk}\cdot\beta^{(2)}_{111}([NO_3]) \\ g_{ijk} &= \sum_{P}^{n}[\alpha(i1)\alpha(j1)\alpha(k1) - \alpha(i1)\alpha(j2)\alpha(k2) \\ &\quad - \alpha(i2)\alpha(j1)\alpha(k2) - \alpha(i2)\alpha(j2)\alpha(k1)] \\ g &= \max(g_{ijk}); \quad (i,j,k = 1,2,3) \end{aligned} \tag{3}$$

In case of unspontaneous polarization, the structural criterion C is defined as:

$$C = \frac{g}{n} \tag{4}$$

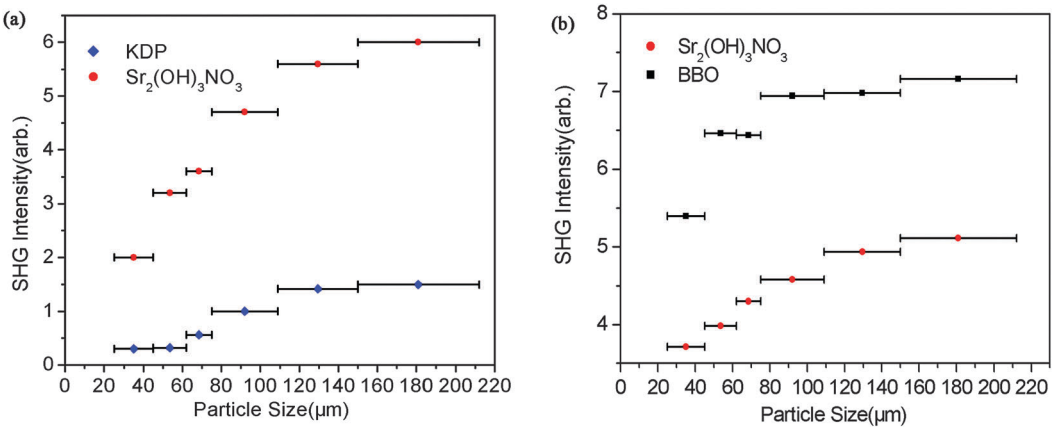

Fig. 4 SHG measurements of ground $Sr_2(OH)_3NO_3$ crystals (red solid circles) and KDP (blue diamonds) as references with the laser at 1064 nm wavelength (a), and SHG measurements of ground $Sr_2(OH)_3NO_3$ crystals (red solid circles) and BBO (black squares) as references with the laser at 532 nm wavelength (b).

where n is the number of anionic groups in a unit cell. So the NLO coefficient $\chi^{(2)}_{ijk}$ is proportional to the density of the $[NO_3]^-$ group (n/V) and the structural criterion (C). Following the computing method used previously[30,43] the calculated value of the C factor for $Sr_2(OH)_3NO_3$ is 100%. The high C factor of $Sr_2(OH)_3NO_3$ arises from its optimized arrangement of the $[NO_3]^-$ groups in the structure (Fig. 1). To gain further insight into the SHG effects as determined by the arrangement of the NLO-active groups and the density of NLO-active groups, the coefficient of the NLO effect for $Sr_2(OH)_3NO_3$ was calculated and compared with the synthesized hydroxide nitrate NLO materials (Table 2). Though the density of $[NO_3]^-$ in $Sr_2(OH)_3NO_3$ is the smallest of the four NLO crystals, the largest structural criterion C leads to the strongest SHG coefficient. Even a moderate density (n/V = 0.0075 Å^{-3}) of $[NO_3]^-$ and large structural criterion values of C factors (100%) lead to the strong NLO effect of $Sr_2(OH)_3NO_3$. As shown in Table 2, the above argument on the structure–property correlations is in good agreement with the SHG measurement.

Theoretical calculations

The band structure is presented in the ESI,† Fig. S5. Compound $Sr_2(OH)_3NO_3$ exhibits an indirect band gap of 5.009 eV. The calculated value is smaller than the experimental value (>6.2 eV) because of the common underestimation of the band gap by the DFT method. The total and partial densities of states (DOS and PDOS) for $Sr_2(OH)_3NO_3$ are presented in Fig. 5. Because the linear-optical and NLO properties are mainly determined by the states close to the Fermi energy level, we discuss only the upper region of the valence band and the bottom of the conduction band. At the energy range between −5 eV and the Fermi level, the

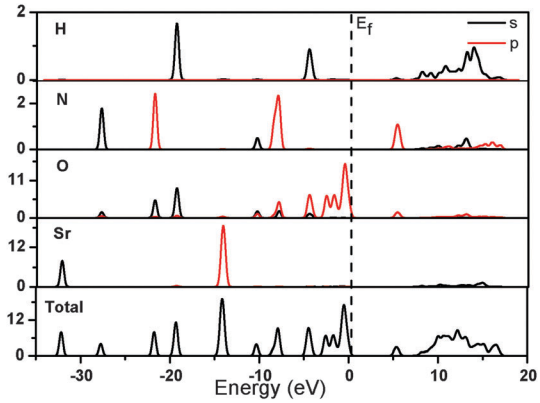

Fig. 5 Total and partial density of states of $Sr_2(OH)_3NO_3$.

DOS is mainly composed of the p orbital of $[NO_3]^-$. The conduction bands from the Fermi level to 7 eV are mainly composed of the p orbital of the $[NO_3]^-$ groups. Thus, the electron transition is mainly contributed by inside excitation of the $[NO_3]^-$ group. Because of the above analysis, the NLO effect of $Sr_2(OH)_3NO_3$ mainly stems from the $[NO_3]^-$ groups, and the perfect spatial arrangement and relatively high density of $[NO_3]^-$ led to the large NLO effect.

Cation coordination control of planar triangle anionic group alignment to maximize SHG effects in NCS UV crystals

In the compounds containing planar $[AO_3]$ (A = B, C, N) groups, there are several reported structures related to the present one. As $[NO_3]$ groups are in parallel alignment in $Sr_2(OH)_3NO_3$, the same arrangements have been observed: $[BO_3]$ groups in NCS

Table 2 NLO effects of $Sr_2(OH)_3NO_3$, $[Pb_4(OH)_4](NO_3)_4$[43], $[LaPb_8O(OH)_{10}(H_2O)](NO_3)_7$[59] and $[LaPb_8O(OH)_{10}(H_2O)](NO_3)_7{\cdot}2H_2O$[59]

Crystals	SHG coefficient (visible) (×KDP)	Structual criterion C	Densities of $[NO_3](n/V)$ (Å^{-3})	$(n/V) \times C$ (Å^{-3})
$Sr_2(OH)_3NO_3$	3.6	1.00	0.0075	0.0075
$[Pb_4(OH)_4](NO_3)_4$	0.7	0.17	0.0109	0.0018
$[LaPb_8O(OH)_{10}(H_2O)](NO_3)_7$	1.3	0.32	0.0087	0.0028
$[LaPb_8O(OH)_{10}(H_2O)](NO_3)_7{\cdot}2H_2O$	1.1	0.31	0.0081	0.0025

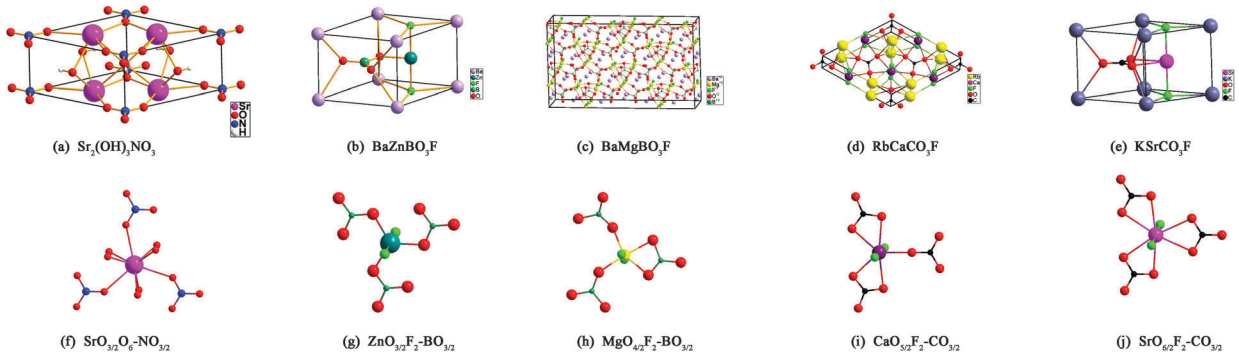

Fig. 6 Alignments of $[AO_3]$ (A = B, C, N) groups by the MO_nF_m polyhedra.

fluoroborates such as $BaZnBO_3F$[45] (Fig. 6b) and $BaMgBO_3F$[45] (Fig. 6c) and $[CO_3]$ groups in NCS fluorocarbonates such as $RbCaCO_3F$[30] (Fig. 6d) and $KSrCO_3F$[30] (Fig. 6e). Though the five compounds have different structures, the main structure units MO_nF_m (n = 3, 4, 5, 6, 9; m = 0, 2) are still strongly correlated, as shown in Fig. 6, All MO_nF_m polyhedra connect to three planar $[AO_3]$ (A = B, C, N) groups by sharing their equatorial oxygen atoms to form MO_n–AO_3 layers. And then two adjacent MO_n–AO_3 layers were connected by the F atoms or O atoms which are situated at the apical positions. From Fig. 6, one can draw a conclusion that the coordination environments strongly affect the structural arrangement of the closest neighboring $[AO_3]$ (A = B, C, N) groups in the crystal. From Fig. 6f–j, the main cation-oxygen (MO_n) coordination number n increases from 3 to 6 at the equatorial positions. In the case of n = 3 or 6, all the M–O bonds pointing to three different $[AO_3]$ (A = B, C, N) groups force them to align in the same orientation (as shown in Fig. 6f, g and j) to give a large NLO contribution, whereas when n = 4 or 5, two of the $[AO_3]$ groups are nearly antiparallel with the other one of the three to cancel out their contributions to the NLO effect (Fig. 6h and i). Following the successful synthesis of a series of NCS compounds with planar triangle structure anionic groups such as borates, carbonates and nitrates, we can work out a principle to design new NCS UV compounds with large nonlinearity: firstly, one needs to choose a basic structure unit that has a large microscopic second-order susceptibility and wide UV transparency, that is, a flat $[AO_3]$ (A = B, C, N) group. And then, select a cation with equatorial oxygen atoms which could force the $[AO_3]$ (A = B, C, N) groups to align parallelly and connect the $[AO_3]$ (A = B, C, N) groups to form a two-dimensional layer, that is, MO_nF_m polyhedra such as a MO_4 tetrahedron or a MO_3F_2 trigonal bipyramid. Third, choose another large cation with nine coordinated atoms in an eclipse style which would possess steric force to arrange the adjacent MO_n–AO_3 layers coparallel to give the maximum contribution to the SHG effect, such as $Sr(OH)_6O_3$ (Fig. 6a), BaO_6F_3 (Fig. 6b), and KO_6F_3 (Fig. 6e). In practice, the controllabilities of the above three rules follow a descending order that the third one is the most difficult to realize.

Conclusions

A noncentrosymmetric nitrate, $Sr_2(OH)_3NO_3$, has been synthesized through a hydrothermal method. In the crystal structure, nine coordinated $SrO_3(OH)_6$ polyhedra and triangular NO_3 groups interconnect *via* sharing corners to form a 3D framework. The $SrO_3(OH)_6$ polyhedra share their three equatorial oxygen atoms with three separate NO_3 groups to form SrO_3–NO_3 layers, and the layers are linked by the apical oxygen atoms in the third dimension. Within a single SrO_3–NO_3 layer, the cooperative connection of triangular SrO_3 and triangular NO_3 makes all NO_3 groups align parallel in the a–b plane and orient in the same direction, giving the maximum contribution to a large macroscopic SHG effect. Second harmonic generation measurement indicates that $Sr_2(OH)_3NO_3$ features a large SHG response that is approximately 3.6 × KH_2PO_4. The result from the UV-vis diffuse reflectance spectroscopy study of the powder samples indicated that the short-wavelength absorption edge was below 200 nm, suggesting that $Sr_2(OH)_3NO_3$ is the first nitrate as a promising deep-UV nonlinear optical material. The growth of large crystals for further physical property studies is ongoing.

Acknowledgements

This research was supported by the National Natural Science Foundation of China (No. 21401178 and 91222204).

Notes and references

1 P. Becker, *Adv. Mater.*, 1998, **10**, 979.
2 P. S. Halasyamani and K. R. Poeppelmeier, *Chem. Mater.*, 1998, **10**, 2753.
3 H. S. K. Ra, K. M. Ok and P. S. Halasyamani, *J. Am. Chem. Soc.*, 2003, **125**, 7764.
4 R. E. Sykora, K. M. Ok, P. S. Halasyamani and T. E. Albrecht-Schmitt, *J. Am. Chem. Soc.*, 2002, **124**, 1951.
5 E. O. Chi, K. M. Ok, Y. Porter and P. S. Halasyamani, *Chem. Mater.*, 2006, **18**, 2070.
6 W. L. Zhang, W. D. Cheng, H. Zhang, L. Geng, C. S. Lin and Z. Z. He, *J. Am. Chem. Soc.*, 2010, **132**, 1508.
7 H. Ye, D. Fu, Y. Zhang, W. Zhang, R. G. Xiong and S. D. Huang, *J. Am. Chem. Soc.*, 2009, **131**, 42.
8 S. C. Wang, N. Ye, W. Li and D. Zhao, *J. Am. Chem. Soc.*, 2010, **132**, 8779.
9 S. C. Wang and N. Ye, *J. Am. Chem. Soc.*, 2011, **133**, 11458.

10 Y. Z. Huang, L. M. Wu, X. T. Wu, L. H. Li, L. Chen and Y. F. Zhang, *J. Am. Chem. Soc.*, 2010, **132**, 12788.
11 F. Kong, S. P. Huang, Z. M. Sun, J. G. Mao and W. D. Cheng, *J. Am. Chem. Soc.*, 2006, **128**, 7750.
12 H. Y. Chang, S. H. Kim, P. S. Halasyamani and K. M. Ok, *J. Am. Chem. Soc.*, 2009, **131**, 2426.
13 C. F. Sun, C. L. Hu, X. Xu, J. B. Ling, T. Hu, F. Kong, X. F. Long and J. G. Mao, *J. Am. Chem. Soc.*, 2009, **131**, 9486.
14 S. L. Pan, J. P. Smit, B. Watkins, M. R. Marvel, C. L. Stern and K. R. Poeppelmeier, *J. Am. Chem. Soc.*, 2006, **128**, 11631.
15 S. W. Bae, C. Y. Kim, D. W. Lee and K. M. Ok, *Inorg. Chem.*, 2014, **53**, 11328.
16 Y. Inaguma, M. Yoshida and T. Katsumata, *J. Am. Chem. Soc.*, 2008, **130**, 6704.
17 D. Phanon and I. Gautier-Luneau, *Angew. Chem., Int. Ed.*, 2007, **46**, 8488.
18 C. T. Chen, *Sci. Sin. (Engl. Ed.)*, 1979, **22**, 756.
19 C. T. Chen and G. Z. Liu, *Annu. Rev. Mater. Sci.*, 1986, **16**, 203.
20 C. T. Chen, Y.C. Wu and R. K. Li, *Int. Rev. Phys. Chem.*, 1989, **8**, 65.
21 C. T. Chen, B. C. Wu, A. D. Jiang and G. M. You, *Sci. Sin., Ser. B*, 1985, **28**, 235.
22 C. T. Chen, Y.C. Wu, A. D. Jiang, B. C. Wu, G. M. You, R. K. Li and S. J. Lin, *J. Opt. Soc. Am. B*, 1989, **6**, 616.
23 Y.C. Wu, T. Sasaki, S. Nakai, A. Yokotani, H. G. Tang and C. T. Chen, *Appl. Phys. Lett.*, 1993, **62**, 2614.
24 Y. Mori, I. Kuroda, S. Nakajima, T. Sasaki and S. Nakai, *Appl. Phys. Lett.*, 1995, **67**, 1818.
25 J. M. Tu and D. A. Keszler, *Mater. Res. Bull.*, 1995, **30**, 209.
26 L. Mei, Y. Wang, C. Chen and B. Wu, *J. Appl. Phys.*, 1993, **74**, 7014.
27 C. T. Chen, Y. B. Wang, B. C. Wu, K. C. Wu, W. L. Zeng and L. H. Yu, *Nature*, 1995, **373**, 322.
28 Z. G. Hu, T. Higashiyama, M. Yoshimura, Y. K. Yap, Y. Mori and T. Sasaki, *Jpn. J. Appl. Phys.*, 1998, **37**, 1093.
29 R. Komatsu, *Appl. Phys. Lett.*, 1997, **70**, 3492.
30 G. H. Zou, N. Ye, L. Huang and X. S. Lin, *J. Am. Chem. Soc.*, 2011, **133**, 20001.
31 G. H. Zou, L. Huang, N. Ye, C. S. Lin, W. D. Cheng and H. Huang, *J. Am. Chem. Soc.*, 2013, **135**, 18560.
32 M. Luo, G. H. Zou, N. Ye, C. S. Lin and W. D. Cheng, *Chem. Mater.*, 2013, **25**, 3147.
33 M. Luo, G. H. Zou, N. Ye, C. S. Lin and W. D. Cheng, *CrystEngComm*, 2014, **16**, 4414.
34 M. Luo, G. X. Wang, N. Ye, C. S. Lin and W. D. Cheng, *Inorg. Chem.*, 2014, **53**, 8098.
35 T. T. Tran and P. S. Halasyamani, *Inorg. Chem.*, 2013, **52**, 2466.
36 T. T. Tran, P. S. Halasyamani and J. M. Rondinelli, *Inorg. Chem.*, 2014, **53**, 6241.
37 C. P. Wang, Q. Liu and Z. H. Li, *Cryst. Res. Technol.*, 2011, **46**, 655.
38 P. Held, H. Hellwig, S. Ruhle and L. Bohaty, *J. Appl. Crystallogr.*, 2000, **33**, 372.
39 L. Bohatý and P. Becker, *Cryst. Res. Technol.*, 2009, **44**, 1131.
40 D. F. Xue and S. Y. Zhang, *Mol. Phys.*, 1998, **93**, 411.
41 C. A. Ebbers, L. D. DeLoach, M. Webb, D. Eimerl, S. P. Velsko and D. A. Keszler, *IEEE J. Quantum Electron.*, 1993, **29**, 497.
42 L. X. Chang, L. Wang, S. L. Pan, R. Hailili, H. W. Yu and Z. H. Yang, *Inorg. Chem.*, 2014, **53**, 3320.
43 G. X. Wang, M. Luo, N. Ye, C. S. Lin and W. D. Cheng, *Inorg. Chem.*, 2014, **53**, 5222.
44 R. K. Li, *Exploration research on inorganic UV nonlinear optical crystal [D]*, Fujian Institute of Research on the Structure of Matter, 1988.
45 R. K. Li and P. Chen, *Inorg. Chem.*, 2010, **49**, 1561.
46 G. M. Sheldrick, *Acta Crystallogr., Sect. A: Found. Crystallogr.*, 2008, **64**, 112.
47 A. L. Spek, *J. Appl. Crystallogr.*, 2003, **36**, 744.
48 P. Kubelka and F. Z. Munk, *Tech. Phys.*, 1931, **12**, 593.
49 J. Tauc, *Mater. Res. Bull.*, 1970, **5**, 721.
50 S. K. Kurtz and T. T. Perry, *J. Appl. Phys.*, 1968, **39**, 3798.
51 M. D. L. Segall, J. D. Philip, M. J. Probert, C. J. Pickard, P. J. Hasnip, S. J. Clark and M. C. Payne, *J. Phys.: Condens. Matter*, 2002, **14**, 2717.
52 J. P. Perdew, K. Burke and M. Ernzerhof, *Phys. Rev. Lett.*, 1996, **77**, 3865.
53 S. Dill, K. Gibson, J. Glaser and H. J. Meyer, *Z. Anorg. Allg. Chem.*, 2007, **633**, 274.
54 M.-H. Choi, S.-H. Kim, H. Y. Chang, P. S. Halasyamani and K. M. Ok, *Inorg. Chem.*, 2009, **48**, 8376.
55 K. M. Ok, J. Baek, P. S. Halasyamani and D. O'Hare, *Inorg. Chem.*, 2006, **45**, 10207.
56 F. Y. Zhang, F. F. Zhang, S. L. Pan and Z. H. Yang, *J. Mater. Chem. C*, 2014, **2**, 667.
57 R. C. Eckardt, H. Masuda, Y. X. Fan and R. L. Byer, *IEEE J. Quantum Electron.*, 1990, **26**, 922.
58 N. Ye, Q. X. Chen, B. C. Wu and C. T. Chen, *J. Appl. Phys.*, 1998, **84**, 555.
59 G. X. Wang, M. Luo, N. Ye, C. S. Lin, Y. Q. Zhou and W. D. Cheng, *Inorg. Chem.*, 2014, **53**, 12584.

